Renormalization group calculation of distribution functions: Structural properties for percolation clusters

J.-P. Hovi [1,2] and Amnon Aharony [1,3]
[1] *Raymond and Beverly Sackler Faculty of Exact Sciences, School of Physics and Astronomy, Tel Aviv University, Ramat Aviv 69978, Tel Aviv, Israel*
[2] *Laboratory of Physics, Helsinki University of Technology, 02150 Espoo, Finland*
[3] *Department of Physics, University of Oslo, P.O. Box 1048, Blindern, N-0316 Oslo 3, Norway*
(Received 21 January 1997)

Distribution functions of properties of critical percolation clusters are calculated using the ''H-cell'' real space renormalization group (RG). We consider structural properties which span two terminals on percolation clusters. These include the lengths of (minimal, average edge-to-edge, longest) self-avoiding walks, the number of the singly connected bonds, and the masses of percolation clusters, as well as of the backbone. We show that the RG corresponds to a (Galton-Watson) branching process, and apply theorems developed in the mathematical literature. We derive recursion relations for the distribution functions, and find exact functional forms for their asymptotic tail behavior at both small and large arguments. The results for the minimal paths have implications on the (multifractal) distribution of wave functions, while the singly connected bonds determine the moments of Ising correlations on these clusters. Our results compare well with existing simulation data. [S1063-651X(97)13806-5]

PACS number(s): 64.60.Ak, 05.70.Jk

I. INTRODUCTION

Consider two points on a random fractal, at a Euclidean distance L from each other. Many physical properties depend on the detailed geometry of the fractal network which connects these two ''terminals.'' For example, the wave functions of localized vibrational excitations or of electrons decay as $\exp(-l/\xi)$, where $l(L)$ is the length of the minimal path (or ''chemical distance'') between the terminals on the network [1,2]. Ising spin correlations decay at low temperatures as $\exp(-l_{sc}/\xi)$, where $l_{sc}(L)$ counts the singly connected bonds on this path [3]. Heisenberg spin correlations decay as $\exp(-R/\xi)$, where $R(L)$ is the ''resistance'' between the ends, when each bond represents a unit resistor [3].

On Euclidean spaces, the geometrical properties l, l_{sc}, and R, as well as many other lengths which determine physical properties, are simply and uniquely expressed in terms of L. For example, $l \propto L$. On regular hierarchical fractals, like the Mandelbrot-Given curve [4], properties like l, l_{sc}, and R have unique power-law dependences on L when the two end points are at the ends of the basic iteration [5], e.g., $l=L$, or $l_{sc}=L^{d_{sc}}$, with $d_{sc}=\ln 2/\ln 3$. If the end points are not at such ends, then the prefactor in this power law may oscillate with L, reflecting lacunarity [6–8].

In the present paper we are concerned with *random fractals*, like percolation clusters at the percolation threshold. For such fractals, quantities like $l(L)$ have different values for different pairs of end points and for different realizations of the random structure. At first, research concentrated on finding the *typical* or the *average* values of such quantities, and it was found that these scale as powers of L, e.g., $\langle l \rangle \propto L^{d_{min}}$ [9].

Here we study *distribution functions*, like $P(l,L)$, where $P(l,L)dl$ represents the probability to measure a shortest path in the range $[l,l+dl]$ for a fixed Euclidean distance L, when the end points cover all possible pairs on all the realizations. Numerically, it has been noted [10,11] that, for large l and L, $P(l,L)$ obeys scaling, i.e.,

$$P(l,L)=\frac{1}{l}g(l/\langle l \rangle). \tag{1}$$

Heuristic arguments also yielded some functional forms for the scaling function $g(\omega)$ [10,12,13]. However, there has been no analytic derivation for Eq. (1), or any exact argument from which the explicit functional form of $g(\omega)$ could be derived. Such arguments are presented below.

As noted above, some physically relevant quantities are exponential in properties like l. For example, localized wave functions behave as $\Psi \propto \exp(-l/\xi)$. The distribution of Ψ is very broad, and moments of Ψ were found to be characterized by independent powers of $\langle \Psi \rangle$ [2]. This phenomenon is called multifractality. Here we extend earlier conclusions on such multifractality, and present results for negative moments. We also derive results for positive and negative moments of the Ising spin correlations.

Our specific calculation concentrates on percolation clusters [5]. At the percolation threshold, these clusters are statistically self-similar. Therefore, they can be described by the renormalization group (RG). Here we use an approximate real space RG, called the ''H cell,'' which turned out to be very accurate for bond percolation on the square lattice [14,15]. It has also given excellent results for the permeability of oil reservoirs, away from the percolation threshold [16]. The H-cell RG is described in Sec. II. Basically, it maps groups of bonds onto renormalized bonds, as shown in Fig. 1. Effectively, each renormalized bond may be described as a ''Wheatstone bridge,'' as shown in Fig. 1(c). Iteration of this mapping is equivalent to replacing the original lattice by a hierarchical structure, in which each bond has an internal structure which is the same as that of the original

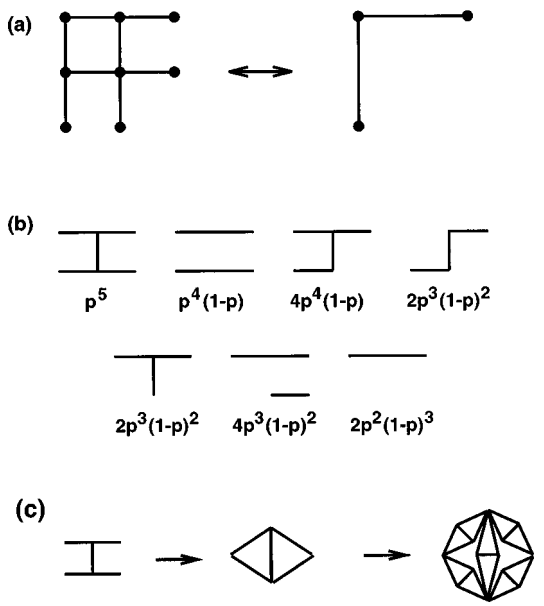

FIG. 1. (a) A 2×2 H cell with eight bonds (left), and a renormalized cell with only two bonds (right), (b) generic parts of the original cell, which contribute to the horizontal spanning, and (c) hierarchical structure for the backbone.

''bridge.'' The H-cell RG equations become exact on this hierarchical lattice. Experience shows [5] that the dilute version of this hierarchical structure imitates the geometrical and physical properties of two dimensional (2D) percolation clusters very well. However, so far this mapping was only used to calculate average properties. Guided by this experience we report the results from the first RG calculation of the full distribution functions. A preliminary brief report of these results appeared in Ref. [17]. As we show below, the calculation of such distribution functions also becomes exact on the hierarchical structure related to the H-cell RG.

When one looks at geometrical properties, we show in Sec. II that the H-cell RG corresponds to a *branching process*. Such processes have been widely studied in the mathematical literature, and in Sec. III we summarize the relevant theorems. These are then used in Sec. IV to study the distributions of the minimal and maximal paths, of average edge-to-edge self-avoiding walks (SAW), of the number of the singly connected bonds, and of the masses of the percolation clusters and of their backbone between the two terminals. Mathematical theorems for the branching processes allow us to derive explicit expressions for the asymptotic tail behavior of the corresponding probability densities, relating the tail behavior to the appropriate fractal dimension. Since the mathematical theorems apply also to the moment generating function $\langle\exp(s\omega)\rangle$, we are also able to derive exact expressions for the (multifractal) moments of functions like Ψ, or Ising spin correlations (Sec. IV D). Finally, a short conclusion completes the paper in Sec. V.

II. ''H-CELL'' RENORMALIZED GROUP

In this section we discuss the RG calculation of various structural properties of percolation clusters. The main result here is the formulation of the RG calculation in terms of a *generating function* f. This formulation enables us to map the RG procedure to the branching processes, which are discussed in Sec. III.

For simplicity, we discuss two dimensional percolation, and consider first a 2×2 H cell, which is shown in Fig. 1(a). In the RG transformation the eight bonds in the cell are replaced by a ''renormalized'' cell with only two bonds, which represent connectivity in the horizontal and vertical directions. Considering the horizontal spanning, and ignoring the dangling bonds, one realizes that the horizontal connectivity is determined by five bonds. Given that each of these five bonds has a probability p $(1-p)$ to be occupied (vacant), the resulting configurations are displayed in Fig. 1(b) together with their probabilities. The sum of these probabilities yields the renormalized probability of the new bond [14,5],

$$p'=R(p)=2p^5-5p^4+2p^3+2p^2. \tag{2}$$

This recursion relation has the nontrivial fixed point $p_c=1/2$, as it should be for the bond problem. One of the advantages of the H cell is that this result holds for a general $L\times L$ cell [15].

Considering the minimal paths we find that only the rightmost configuration in the upper row of Fig. 1(b) has a minimal path length $l=3$, while all other spanning configurations have $l=2$. At p_c, we thus have $l=3$ with probability $p_3=2p^3(1-p)^2/p'=1/8$, and $l=2$ otherwise, with $p_2=7/8$. Averages of l within a cell can be calculated from the generating function

$$f_{\min}(z)=p_2z^2+p_3z^3. \tag{3}$$

Specifically,

$$\langle l^k\rangle=2^kp_2+3^kp_3=\left(z\frac{d}{dz}\right)^k f_{\min}(z)\big|_{z=1}, \tag{4}$$

and $\langle l\rangle=f'_{\min}(1)=\mu_{\min}=17/8$.

Similar considerations on the H-cell RG can be extended for several other structural properties, like the maximal paths (longest SAW between the edges), the average length of all the edge-to-edge SAW's, the number of the singly connected bonds (SCB), and the mass of the backbone (BB):

$$f_{\max}(z)=\tfrac{9}{16}z^2+\tfrac{7}{16}z^3, \tag{5}$$

$$f_{\text{saw}}(z)=\tfrac{23}{32}z^2+\tfrac{9}{32}z^3, \tag{6}$$

$$f_{\text{sc}}(z)=\tfrac{1}{8}+\tfrac{2}{8}z+\tfrac{4}{8}z^2+\tfrac{1}{8}z^3, \tag{7}$$

$$f_{\text{bb}}(z)=\tfrac{8}{16}z^2+\tfrac{2}{16}z^3+\tfrac{5}{16}z^4+\tfrac{1}{16}z^5, \tag{8}$$

with $\mu_{\max}=39/16$, $\mu_{\text{saw}}=73/32$, $\mu_{\text{sc}}=13/8$, and $\mu_{\text{bb}}=47/16$, respectively. Note that for the average edge-to-edge SAW (f_{saw}) every SAW is considered to be equally probable, irrespective of its actual length. This corresponds to the infinite temperature limit, where the fugacities are equal for all the bonds. For alternative approaches see, e.g., Refs. [18] and [19]. The generating function for the mass of the backbone is given by calculating the number of bonds which support SAW. The mass of the percolation cluster at p_c is determined by the spanning configurations of the complete eight bond cell, from which we find that

TABLE I. Estimates for the fractal dimensions from the RG calculations with the length rescale factor $L=2,3,4$. The rightmost entry is the exact result (or numerical estimate if the exact value is unknown).

Property	$L=2$	$L=3$	$L=4$	$L\to\infty$
singly connected bonds (d_{sc})	0.700	0.725	0.734	3/4 [21]
minimal path (d_{min})	1.087	1.118	1.133	1.14 ± 0.01 [11,22]
average edge-to-edge SAW (D_{saw})	1.190	1.243	1.268	1.29 ± 0.025 [23–25]
maximal path (d_{max})	1.285	1.357	1.389	1.4 ± 0.1 [5]
mass of backbone (D_{bb})	1.555	...	...	1.647 ± 0.004 [26]
mass of the cluster (D)	2.155	1.979	1.928	$91/48\approx1.896$ [5]

$$f_{\text{mass}}(z)=\tfrac{15}{128}z^2+\tfrac{18}{128}z^3+\tfrac{31}{128}z^4+\tfrac{32}{128}z^5+\tfrac{23}{128}z^6+\tfrac{8}{128}z^7+\tfrac{1}{128}z^8 \tag{9}$$

yielding $\mu_{\text{mass}}=285/64$.

These functions f are completely determined by the RG. In order to calculate them one has to classify all possible spanning configurations of the renormalized cell. The time required for this classification increases very rapidly with increasing cell size. However, the lowest and highest order terms in the polynomial f are easy to deduce: for a general $L\times L$ cell one has

$$f(z)=p_m z^m+\cdots+p_M z^M, \tag{10}$$

where $m=0$ for SCB, and $m=L$ otherwise, while $M=2L^2$ for f_{mass}, but $M=(L-1)^2+L$ for all the other cases. It is shown in Sec. III, that knowing the lowest and highest order terms is enough to determine the tail behavior of the relevant distributions.

We next consider the renormalization of the function $f(z)$, for example, f_{min}. It is easy to see that since each cell can have $l=2$ or $l=3$, at the next iteration the larger cell will have all the values from $l=2^2=4$ to $l=3^2=9$, with corresponding binomial coefficients. It follows that the renormalized generating function $f^{(2)}$ has the form

$$f^{(2)}(z)=f[f(z)], \tag{11}$$

for example,

$$f^{(2)}_{\text{min}}(z)=p_2(p_2z^2+p_3z^3)^2+p_3(p_2z^2+p_3z^3)^3. \tag{12}$$

After n iterations the generating function is determined via the recursion relation

$$f^{(n)}(z)=f[f^{(n-1)}(z)]=f^{(n-1)}[f(z)], \tag{13}$$

and $f^{(n)}_{\text{min}}(z)$ is a polynomial with powers from 2^n to 3^n. Equation (13) expresses mathematically the basic spirit of the H-cell RG. As stated, this procedure maps the original lattice onto a hierarchical structure, whose backbone is built on the basic Wheatstone bridge [5,19] [see Fig. 1(c)]. On this hierarchical structure, each bond splits into smaller bonds independently of the other bonds, ending up with the binomial coefficients as in Eq. (12), with multiplicative probabilities (e.g., p_2^3 to have four bonds on the minimal path after two iterations). This binomial multiplicative process, which is a dominant ingredient of the hierarchical structure, is the basis for our mathematical analysis below.

Indeed, iterating f, say f_{min}, one observes that the average minimal path length increases in a multiplicative fashion. The average $\langle l\rangle$ after n iterations becomes

$$\langle l\rangle_n=\left.\frac{df^{(n)}(z)}{dz}\right|_{z=1}=f'(1)\left.\frac{df^{(n-1)}(z)}{dz}\right|_{z=1}=\mu_{\text{min}}^n, \tag{14}$$

because $f^{(n)}(1)=1$ for all n. Since the end-to-end length is $L=2^n$, we conclude that $\langle l\rangle_n=L^{d_{\text{min}}}$, with $d_{\text{min}}=\ln(\mu_{\text{min}})/\ln(2)\approx1.087$, as found before from this RG [20].

Similarly, we find the estimates for the dimensions of other structural properties. These results are collected in Table I, together with the exact results, or numerical estimates if the exact value is unknown. Typically, the estimates from the 2×2 H cell deviate from the best estimates by 10%. As shown in Table I, the agreement can, however, be considerably improved by repeating the calculations with a larger $L\times L$ cell. For example, the RG results from cells with $L=4$ (full cell having 32 bonds, out of which 25 bonds determine the horizontal connectivity—a relatively small system still), are within 1% of the best estimates.

To appreciate the general validity of the present approach, we consider the kth moment of, say, l. This is given by

$$\langle l^k\rangle_n=\left.\frac{d^kf^{(n)}(z)}{d(\ln z)^k}\right|_{z=1}=\mu^k\left.\frac{d^kf^{(n-1)}(z)}{d(\ln z)^k}\right|_{z=1}+\cdots=\mu_{\text{min}}^{kn}+\cdots=L^{kd_{\text{min}}}+\text{corrections}. \tag{15}$$

Thus the RG calculations, as presented here, are applicable for general *unifractal* distributions, which have the common feature that $f(z)$ is analytical, being a simple polynomial with only integer powers of z. In particular, Sec. III deals with mathematical branching processes, which assume that the probability generating function f is analytical. A drawback is that our discussion excludes the distribution of resistances, for which one would find nonanalytical $f_R(z)$, e.g., 2×2 H cell gives

$$f_R(z)=\tfrac{1}{8}z+\tfrac{2}{8}z^{5/3}+\tfrac{4}{8}z^2+\tfrac{1}{8}z^3, \tag{16}$$

with $\mu_R=23/12$.

III. BRANCHING PROCESSES

Consider again the minimal paths in the H-cell RG with $b=2$. As discussed in Sec. II, each bond on the minimal path

has the same branching probabilities, p_2 and p_3, to split into two or three smaller steps, respectively. This defines a random process with the probability generating function $f(z)$ [see Eq. (3), which obeys Eq. (13)]. The mathematical literature identifies these kinds of random processes as (Galton-Watson) branching processes [27]. The same applies to the other properties discussed above. Therefore, we now summarize some existing exact results concerning these processes, which we use in Sec. IV. For more details see Ref. [27] and articles cited below.

The mathematical branching process originates from a study of the family extinction [28]. The probability that a parent has exactly r children is p_r, $r=0,1,2,\ldots$. Each individual in the following generations has the same probabilities of having a certain number of off-springs. The number of members in the nth generation is X_n, and the aim is to study the probability distribution of X_n as $n\to\infty$. The connection to the H-cell RG calculations for distributions of structural properties, as described in Sec. II, is quite clear.

Indeed, also in this context the fundamental quantity is the *probability generating function* $f(z)$, which describes how a single individual branches in each generation

$$f(z)=\sum_{r=0}^{\infty} p_r z^r = p_m z^m + \cdots + p_M z^M, \tag{17}$$

where $m(M)$ is the minimum (maximum) number of offsprings, and z is a complex auxiliary variable. The mean number of the offsprings is $\mu=f'(1)$. Depending on μ, the branching process is supercritical ($\mu>1$), critical ($\mu=1$), or subcritical ($\mu<1$). While μ is related to the fractal dimensionality $\widetilde{D}$ via $\mu=L^{\widetilde{D}}$, these correspond to $\widetilde{D}>0$, $\widetilde{D}=0$, and $\widetilde{D}<0$, respectively. In this paper, we need to consider only the supercritical branching processes.

For what follows it is essential that we have a finite $\mu>1$, i.e., a *supercritical* process. It is easy to check that this condition is valid for all the cases of the preceding section. For the supercritical branching process one can show [27] that the population size normalized by the mean number of the offsprings, $\omega_n=X_n/\mu^n$, converges (as $n\to\infty$) almost surely (everywhere, except on a set of zero measure) to a nondegenerate limit distribution $g(\omega)\equiv\lim_{n\to\infty} f^{(n)}(\omega\mu^n)$. This mathematical proof [27] thus also confirms that $g(\omega)$ is only a function of the scaled variable $\omega=X/\langle X\rangle$, proving the scaling form Eq. (1) for this type of RG. In order to study g, define the *moment-generating function* $\phi(s)$ by

$$\phi(s)\equiv\langle e^{\omega s}\rangle=\int e^{\omega s} g(\omega)\,d\omega. \tag{18}$$

Of course, the knowledge of $\phi(s)$ is sufficient to determine the probability density of the limit distribution, because $g(\omega)$ is given by Fourier transforming $\phi(it)$ (with real t). Next we derive an equation for ϕ. Using the relation

$$\langle X^k\rangle=\left(z\frac{d}{dz}\right)^k f(z)\big|_{z=1}=\left(\frac{d}{d(\ln z)}\right)^k f(z)\big|_{z=1}, \tag{19}$$

it follows that

$$\langle e^{sX}\rangle=\sum_k \frac{s^k}{k!}\langle X^k\rangle=\sum_k \frac{s^k}{k!}\left(\frac{d}{d(\ln z)}\right)^k f(z)\big|_{z=1}$$
$$=f(e^{\ln z+s})\big|_{z=1}=f(e^s). \tag{20}$$

Therefore, after the first iteration we have

$$\phi^{(1)}(s)=\langle e^{sX/\langle X\rangle}\rangle=f(e^{s/\langle X\rangle}). \tag{21}$$

After n iterations, $\langle X\rangle_n=\mu^n$ [see also Eq. (14)], and thus

$$\phi^{(n)}(\mu s)=f^{(n)}(e^{s/\mu^{n-1}})=f[f^{(n-1)}(e^{s/\mu^{n-1}})]$$
$$=f[\phi^{(n-1)}(s)]. \tag{22}$$

Since $\phi^{(n)}(s)$ has a limit $\phi(s)$ for $n\to\infty$, this yields

$$\phi(\mu s)=f[\phi(s)], \tag{23}$$

from which ϕ, and thus also g, can be determined for given f. Below we use this procedure to derive $g(\omega)$ for the distributions discussed in earlier sections.

From Eqs. (17) and (23) one can derive very useful asymptotic laws for the moment-generating function $\phi(s)$ with real s. The first part is due to Harris [29], and the second to Bingham [30].

Theorem 1. Assume that $\mu>1$, and let $\delta=\log_\mu M$, and $\eta=\log_\mu m$. Then

(1) As $s\to\infty$,

$$\ln\phi(s)=s^\delta A(s)+O(1), \tag{24}$$

where $A(s)$ is continuous, positive and periodic in $\ln(s)$; $A(\mu s)=A(s)$.

(2) If $m>1$ in Eq. (17), then as $s\to-\infty$,

$$-\ln\phi(s)=(-s)^\eta B(s)+O(1), \tag{25}$$

where $B(s)$ is continuous, positive and periodic in $\ln(s)$; $B(\mu s)=B(s)$.

(3) If $m\leqslant 1$ in Eq. (17), then as $s\to-\infty$,

$$-\ln\phi(s)=-\alpha s+O(1), \tag{26}$$

where $\alpha=-\log_\mu[f'(q)]$, and q is the smallest non-negative solution for $q=f(q)$.

Theorem 1 yields the following results for the tail behavior of the limit distribution $g(\omega)$. The first two parts, which relate to the cumulative probability density $G(\omega)=\int_0^\omega g(\omega')d\omega'$, are due to Biggins and Bingham [31], while the last part, a local result for g when $m\leqslant 1$, is originally due to Dubuc [32] and sharpened in [31].

Theorem 2. Again $\mu>1$, $\delta=\log_\mu M$, $\eta=\log_\mu m$ [see Eq. (17)], and define the cumulative probability density $G(\omega)=\int_0^\omega g(\omega')d\omega'$. Then

(1) As $\omega\to\infty$,

$$-\ln[1-G(\omega)]=x^{\delta'}A^\dagger(\omega)+o(\omega^{\delta'}), \tag{27}$$

where $\delta'=\delta/(\delta-1)>0$, and $A^\dagger(\omega)$ is real analytic on $(0,\infty)$, positive and multiplicatively periodic with period $\mu^{\delta-1}$; $A^\dagger(\mu^{\delta-1}\omega)=A^\dagger(\omega)$.

(2) If $m>1$ in Eq. (17), then as $\omega\to 0$,

$$-\ln G(\omega)=\omega^{\eta'}B^{\dagger}(\omega)+o(\omega^{\eta'}). \tag{28}$$

where $\eta'=\eta/(\eta-1)<0$, and $B^{\dagger}(\omega)$ is real analytic on $(0,\infty)$, positive and multiplicatively periodic with period $\mu^{1-\eta}$; $B^{\dagger}(\mu^{1-\eta}\omega)=B^{\dagger}(\omega)$.

(3) If $m\leqslant 1$ in Eq. (17), define $\hat{f}(z)=[f(q+(1-q)z)-q]/(1-q)$, where q is the smallest non-negative solution for $q=f(q)$. Then the moment generating function for the conditional probability density $\hat{g}(\omega)\equiv\lim_{n\to\infty}\hat{f}^{(n)}(\omega\mu^{\eta})$, given that $\omega\neq 0$, satisfies Eq. (23) with $\hat{f}$. As $\omega\to 0$,

$$\hat{g}(\omega)=\omega^{\alpha'}C^{\dagger}(\omega)+o(\omega^{\alpha'}), \tag{29}$$

where $\alpha'=\alpha-1$, $\alpha=-\log_{\mu}[f'(q)]=-\log_{\mu}[\hat{f}'(0)]$, and $C^{\dagger}$ is a continuous, positive, and multiplicatively periodic function $C^{\dagger}(\omega)=C^{\dagger}(\mu\omega)$.

In the last part of Theorem 2, which deals with the conditional probability density $\hat{g}(\omega)$, the parameter $q=g(0)=\lim_{n\to\infty}f^{(n)}(0)$ is the probability that $\omega=0$. To see that q is also given by solving $q=f(q)$, consider the recursion relation $f^{(n)}(z)=f[f^{(n-1)}(z)]$. The fact that $q=f(q)$ follows by setting $z=0$ and letting $n\to\infty$. One has to pick the smallest non-negative root because f is a convex function [27].

The previous theorems contain the periodic functions $(A,A^{\dagger},B,B^{\dagger},C^{\dagger})$, which, however, turn out to be practically constants. This near constancy phenomenon is mathematically interesting in its own right, and has been studied in several papers [30–33]. Here it is enough to note that the Fourier coefficients of these periodic functions decay exponentially [32,33]. We have calculated these functions numerically [34] for several cases arising from our small-cell RG calculations, and found that the relative variation of these functions is of the order 10^{-3} at most.

IV. DISTRIBUTIONS OF STRUCTURAL PROPERTIES

We now apply the above considerations to the distributions of geometrical properties on percolation clusters. We introduce the numerical procedure used in solving Eq. (23) for our RG calculations (Sec. IV A 1). Numerically calculated distributions of several structural properties from small-cell RG are compared with the predictions of Theorem 2 for the supercritical branching processes in Secs. IV A 2, IV A 3. While we expect that our RG distributions approach the exact distributions for percolation clusters in the limit $L\to\infty$, we utilize the general structure of the probability generating function f [see discussion after Eq. (10)] to deduce general predictions for the asymptotic tail behavior for both small and large arguments (Sec. IV B). These predictions are then compared with the numerical data from the critical percolation clusters (Sec. IV C).

In the last part of this section (Sec. IV D) we apply our results to the (multifractal) moments of localized wave functions and the Ising spin correlations at low temperatures. These relate to the minimal path and SCB distributions, respectively.

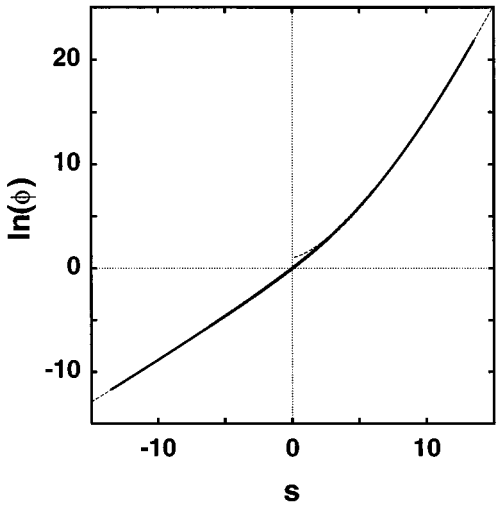

FIG. 2. The moment-generating function $\phi(s)$ (solid line) for the minimal paths calculated from the 2×2 H cell. Dashed lines represent the asymptotic behavior from Theorem 1. As $s\to\infty$, $\ln(\phi)=c_1+As^{\delta}$, and for $s\to-\infty$, $\ln(\phi)=c_2-B(-s)^{\eta}$. From Eqs. (3) and (23) we get for this case $c_1=-\frac{1}{2}\ln(0.125)$, $A\approx 0.4667$, $\delta=\ln(3)/\ln(2.125)$, $c_2=-\ln(0.875)$, $B\approx 1.0817$, $\eta=\ln(2)/\ln(2.125)$.

A. Structural properties of percolation: RG calculations

1. Numerical solution of Eq. (23)

In order to check the mapping between the branching processes and the RG calculations for the distribution functions, we start by solving Eq. (23) for $\phi(s)$ [29], where the probability generating function f is determined by an exact enumeration of H cells with a length rescale factor L (here $L=2,3,4$). For small s, ϕ is analytic, and can be expanded as a Taylor series $\phi(s)=\Sigma a_k s^k$. Substituting into Eq. (23), we can solve for the coefficients $\{a_k\}$ up to a certain order. Having a good approximant for $\phi(s)$ in the range $s_0<|s|<\mu s_0$ near the origin, we then iterate Eq. (23) to find ϕ for larger $|s|$. In this work we typically computed the first 16–24 terms of the Taylor series, and s_0 was chosen in such a way that $\mu s_0\approx 0.7$.

For example, the results for the minimal path case (from the 2×2 H cell) are shown in Fig. 2. Clearly, the results agree well with the asymptotic predictions of Theorem 1, with visible deviations only at small positive s. Having solved Eq. (23) for ϕ, we next derived $g(\omega)$ by Fourier transforming $\phi(it)$ numerically (the real part is an even, and the imaginary part is an odd function). As described in Sec. III, this gives the distribution functions $g(\omega)$ for the small-cell RG calculations. These distribution functions are compared with the asymptotic predictions of Theorem 2 below.

2. Comparison of RG data with asymptotics of Theorem 2: Supercritical case m>1

We consider first the supercritical case $m>1$, which excludes only the number of SCB's. For example, Fig. 3 displays the cumulative distribution functions for (a) minimal paths, (b) average edge-to-edge SAW, and (c) the mass of the percolation cluster calculated from the H-cell RG with $L=2$. The dashed lines in Fig. 3 show the predictions of Theorem 2

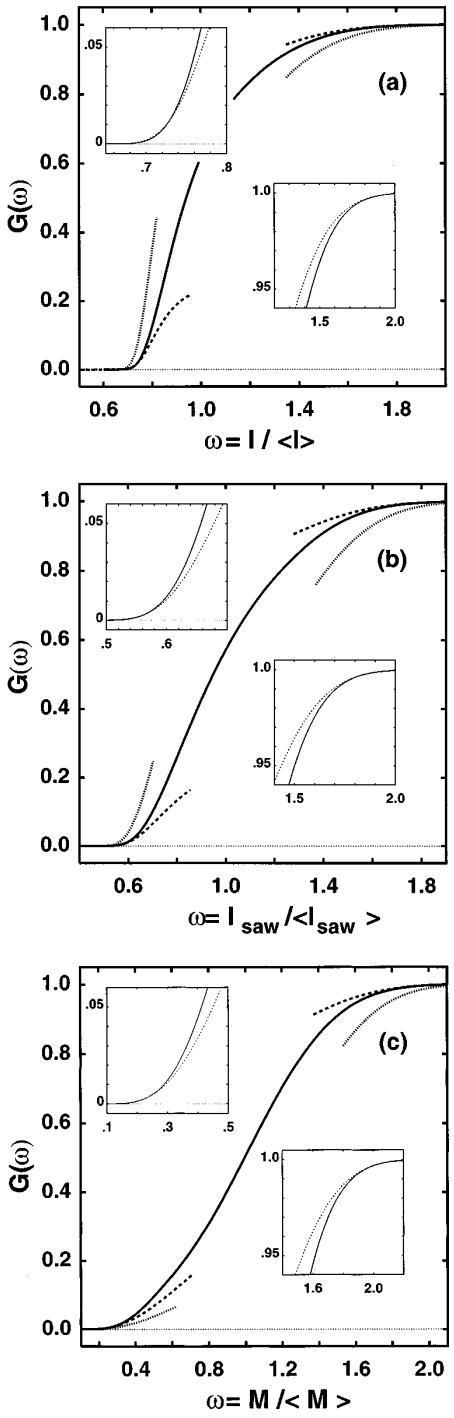

FIG. 3. Cumulative distribution functions for (a) minimal path, (b) average edge-to-edge SAW, (c) mass of the percolating cluster (solid lines). The data are calculated from the H-cell RG with $L=2$. Dashed lines (main chart and insets) show the suggested asymptotic tail behavior Eqs. (30) and (31): for large ω, $1-G(\omega)=c_1'\exp(-A^\dagger\omega^{\delta'})$, while for small ω, $G(\omega)=c_2'\exp(-B^\dagger\omega^{\eta'})$. The proportionality constants $c_{1,2}'$ are fitted to the data, but the rest of the numerical factors are determined by RG: (a) $\delta'\approx 3.186$, $\eta'\approx -11.43$, $A^\dagger\approx 0.7287$, $B^\dagger\approx 0.0818$, $c_{1,2}'=0.38\pm 0.05$, 0.25 ± 0.04, (b) $\delta'\approx 4.011$, $\eta'\approx -5.268$, $A^\dagger\approx 0.4046$, $B^\dagger\approx 0.2183$, $c_{1,2}'=0.28\pm 0.04$, 0.27 ± 0.04, (c) $\delta'\approx 3.550$, $\eta'\approx -0.8659$, $A^\dagger\approx 0.3795$, $B^\dagger\approx 1.796$, $c_{1,2}'=0.28\pm 0.04$, 1.8 ± 0.2. For comparison, dotted lines in the main chart show the fit using $c_1'=c_2'=1$.

$$G(\omega)=c_2'\exp(-B^\dagger\omega^{\eta'}) \quad \text{for } \omega\ll 1, \tag{30}$$

$$1-G(\omega)=c_1'\exp(-A^\dagger\omega^{\delta'}) \quad \text{for } \omega\gg 1. \tag{31}$$

Note that since the first two parts of Theorem 2 give the asymptotic behavior of the cumulative distribution functions only within exponential accuracy, we have allowed constant prefactors $c_{1,2}'$ to stimulate higher order corrections. Figure 3 indicates that such prefactors are enough to achieve a good fit between the data and asymptotic results of Theorem 2 [35].

Although we lack detailed mathematical information on the probability density, we can compare $g(\omega)$ with the derivative of $G(\omega)$. Thus we expect that

$$g(\omega)=-c_2'B^\dagger\eta'\omega^{\eta'-1}\exp(-B^\dagger\omega^{\eta'}) \quad \text{for } \omega\ll 1, \tag{32}$$

$$g(\omega)=c_1'A^\dagger\delta'\omega^{\delta'-1}\exp(-A^\dagger\omega^{\delta'}) \quad \text{for } \omega\gg 1. \tag{33}$$

Of course, the corrections to the exponential terms of Theorem 2 may be the source of power-law prefactors which differ from those of Eqs. (32) and (33). However, while such corrections are presently unknown [35], we compare our data with these equations. Figure 4 shows the distribution functions $g(\omega)$ for (a) minimal paths, (b) average edge-to-edge SAW and (c) the mass of the percolation cluster, as calculated from the H-cell RG with $L=2$. The same figure shows Eqs. (32) and (33) as dashed lines. We find that the data show a good agreement with Eqs. (32) and (33) in both tails, although usually the asymptotic regime is quite far away from the peak of the distribution. This peak is often well described by an asymmetric Gaussian function (see, e.g., Fig. 3 of Ref. [17]).

We also studied these distributions using the H-cell RG with $L=3,4$, as well as the distributions of the maximal path and the mass of the backbone (data not shown). We also found similar results for all these other cases, independent of the length rescale factor L or of the physical property of interest.

In conclusion, Theorem 2 implies that the distribution functions g decay essentially exponentially in both ends, although possibly with more slowly varying prefactors which may involve an unknown power law of ω, another exponential term, or at least a multiplicative constant [35]. Note, however, that Theorem 2 does not identify the ranges of ω for which the asymptotic exponential dependence applies. It is not *a priori* clear if available numerical data reach these ranges.

3. Comparison of RG data with asymptotics of Theorem 2: Supercritical case $m\leqslant 1$

This part applies to the distribution of the number of singly connected bonds. Since f_{sc} has $m=0$ [see Eq. (7)], Theorem 2 implies that the H-cell RG has a nonzero probability to have no SCB. As discussed after Theorem 2, this probability is given by the smallest non-negative root of the equation $q=f_{sc}(q)$. For the $L\times L$ H-cell RG, we find that

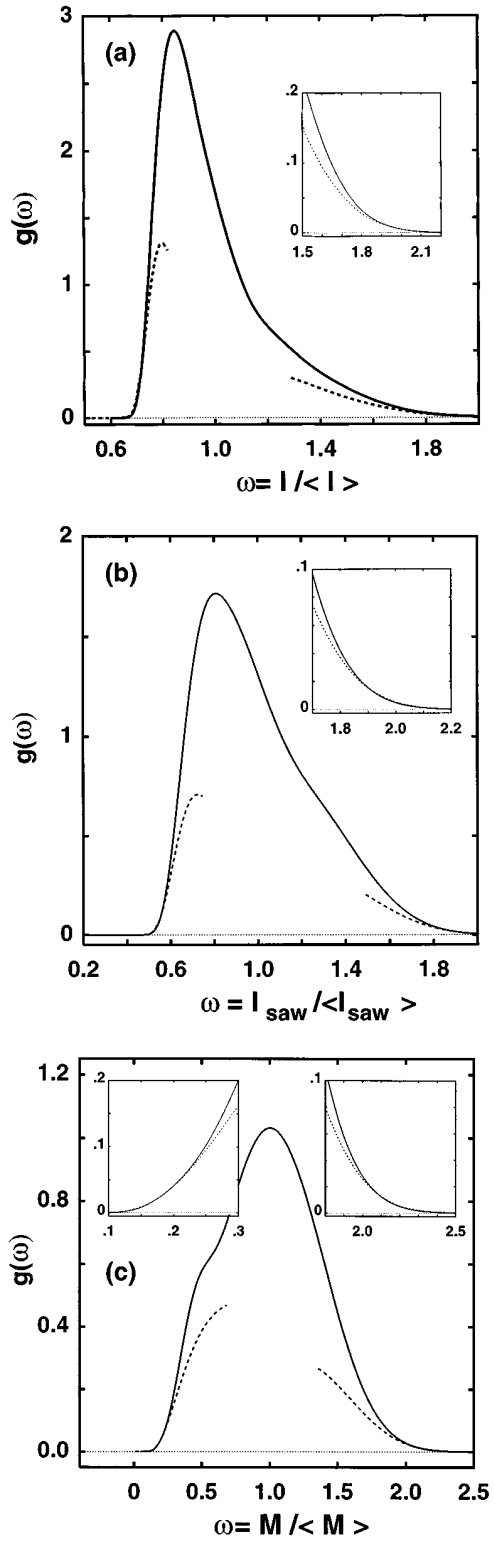

FIG. 4. Distribution $g(\omega)$ for (a) minimal path, (b) average edge-to-edge SAW, and (c) mass of the percolating cluster (solid lines). The data are calculated from the H-cell RG with $L=2$. The dashed lines show the suggested asymptotic tail behavior Eqs. (32) and (33). The numerical factors are the same as in Fig. 3.

$q=g(0)\approx 0.1926, 0.1918, 0.1905$ for $L=2,3,4$, respectively. As discussed below, extrapolation to large L still leaves this fraction at about 18% here.

Because SCB has $g(0)>0$ [contrary to the previous cases above where $g(0)=0$] we shall study the distribution $\hat{g}(\omega)$, i.e., the probability density given that $\omega\neq 0$, instead of g. As $m=0$, the third part of Theorem 2 applies, and we have a local result for the left-hand tail of the $\hat{g}$

$$\hat{g}(\omega)=C^{\dagger}\omega^{\alpha'}, \quad \text{for } \omega\ll 1, \tag{34}$$

while the right-hand tail of $\hat{g}$ is still (at least within exponential accuracy) described by Eq. (33). Equation (34) involves the exponent α', which can be determined by the RG similarly to $d_{sc}=\log_L[\mu]$. Due to the relation $q=f(q)$, one realizes that $f'(q)$ increases multiplicatively, i.e., $(d/dz)f^{(n)}(z)_{|z=q}=[f'(q)]^n$. Therefore, one can define an exponent $x=\log_L[f'(q)]=\alpha d_{sc}$. Calculating x for small cell sizes, we can extrapolate the results to $L\to\infty$ in a somewhat controlled manner. Studying the distributions for cell sizes $L\leqslant 4$, we find that $x\approx 1.1313$, 1.12 447, 1.10 562, i.e., $\alpha'=(x-d_{sc})/d_{sc}\approx 0.6162$, 0.5510, 0.5063, for $L=2,3,4$, respectively (the results for d_{sc} are listed in Table I). Plotting these numbers vs $1/\ln L$ [5] and extrapolating to $L\to\infty$, we estimate $x=1.0\pm 0.1$, which gives $\alpha'=0.35\pm 0.15$.

We now compare the RG data with Eqs. (34) and (33). For example, Fig. 5 shows the results of the RG calculation of $\hat{g}$ from a 2×2 H cell (solid lines), together with the asymptotics of Eqs. (34) and (33) (dashed lines). We also studied the distributions for length rescale factors $L=3,4$, but the results are very similar and therefore the data are not shown. In particular, we find (see, e.g., Fig. 5) that the left-hand tail of the data agrees excellently with Eq. (34). The data also agree with the exponential decay on the right-hand tail, but the asymptotic regime is again quite far away from the peak.

B. Predictions for the tail behavior of the distribution functions in real samples

We expect our RG results to approach the exact distributions for percolation clusters in the limit $L\to\infty$. Furthermore, the scaling function $g(\omega)$ is expected to be universal for every system with the same dimensionality, system shape and boundary conditions. In fact, our renormalization group argument bears this out, showing analytically that g depends only on the scaled variable, e.g., $\omega=l/\langle l\rangle$. Of course, in a real percolation problem the average, say, minimal path is only proportional to $L^{d_{\min}}$, and therefore $l/\langle l\rangle=l/aL^{d_{\min}}$ (the RG has $a=1$). The correct choice of a gives $\langle l/\langle l\rangle\rangle=1$ and normalizes the distribution simultaneously. Details for the specific systems should therefore enter the scaling function only via this nonuniversal amplitude a. Below we use the general structure of the probability generating function f to deduce general predictions for the asymptotic tail behavior of these universal distribution functions.

1. Supercritical case m>1

As explained above, μ is related to the fractal dimension $\tilde{D}$ via $\mu=L^{\tilde{D}}$. For large L, we have $m=L, M\approx L^2$ [see Eq. (10)], and, therefore,

$$\eta=1/\tilde{D}, \tag{35}$$

$$\delta=2\eta, \tag{36}$$

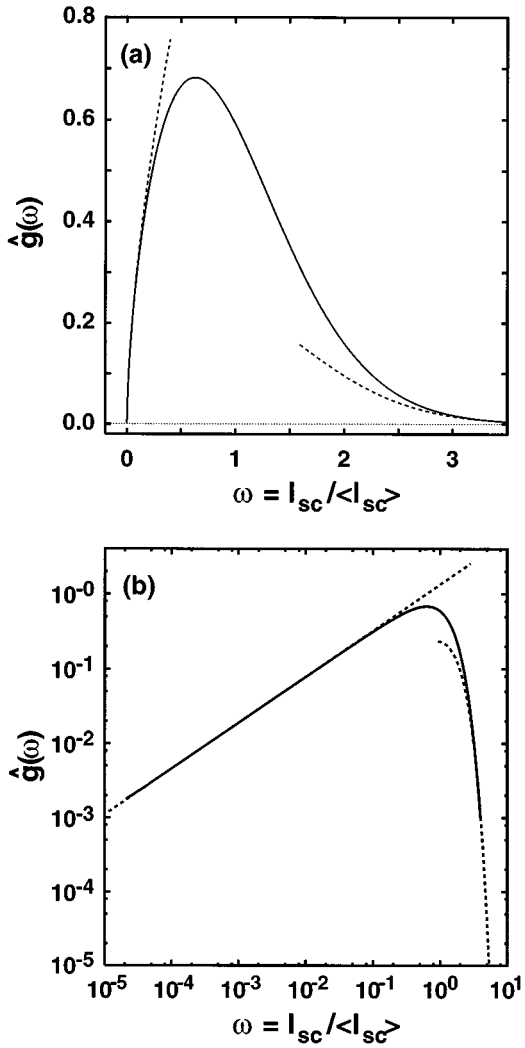

FIG. 5. The conditional probability density $\hat{g}(\omega)$ of the number of the singly connected bonds on (a) linear, (b) double-logarithmic scale (solid lines). The dashed lines show the suggested asymptotic tail behavior Eqs. (34) and (33). The data are calculated form the H-cell RG with $L=2$. In this case we find $C^{\dagger}\approx 1.3345$, $\alpha'\approx 0.6162$, $\delta'\approx 1.792$, $A^{\dagger}\approx 0.5844$, $c_1'=0.4\pm 0.1$.

$$\eta' = (1-\tilde{D})^{-1}, \tag{37}$$

$$\delta' = 2/(2-\tilde{D}). \tag{38}$$

The exponential tail behavior of Eqs. (32) and (33) is, therefore, simply related to the appropriate fractal dimension $\tilde{D}$. These results should hold, e.g., for the distributions of (i) minimal paths, (ii) average edge-to-edge SAW, (iii) maximal paths, (iv) the mass of the percolation cluster, as well as for (v) the mass of the backbone.

2. Supercritical case $m \leqslant 1$

This section applies to the distribution of the singly connected bonds. The RG calculations presented in Sec. IV A 3 reveal three major features, which we expect to hold also for real critical percolation clusters.

(1) There is a finite probability q that the percolation cluster has no SCB. For the H-cell RG this probability is quite large: the small-cell RG calculations give $q\approx 0.18\pm 0.01$ as $L\to\infty$.

(2) For $\omega \ll 1$, Eq. (34) holds, and $\hat{g}$ should be a power law $\hat{g}\propto\omega^{\alpha'}$. As discussed in Sec. IV A 3, α' depends on the details of f, and we do not know how to express it simply in terms of the fractal dimension d_{sc}. It is possible that α' is a new independent exponent. Our numerical RG calculations give $\alpha'=0.35\pm 0.15$ for $L\to\infty$.

(3) For $\omega \gg 1$, g is described (at least within exponential accuracy) by Eq. (33). For this case $\delta'=2/(2-d_{sc})=8/5$.

C. Comparison of the predictions with the numerical data

We are now in the position to compare the predictions from the RG calculations with the numerical data. We start discussing the supercritical case $m>1$, and we concentrate on the distributions of the mass of the cluster and of the minimal paths. One motivation for this choice is that the asymptotics of Eqs. (32) and (33) may dominate the data only quite far away from the peak. This fact is evident also in the RG data (see Sec. IV A), for which one knows that Theorem 2 is exact. Since the numerical data for critical percolation clusters is inevitably less accurate than our small-cell RG calculations, we feel that one should start with easy examples. Our RG considerations imply that because the fractal dimension for the minimal paths (mass of the cluster) is close to 1 (2), $\eta'(\delta')$ is large, and thus most of the weight is on the left- (right-) hand tail of g. Thus the shape of these distributions should make the exponential decay easy to observe on the fastly decaying tail. Unfortunately, the opposite may hold for the other tail.

Furthermore, simulations on real percolation clusters have been usually performed with fixed topological, rather than with fixed geometrical distance [10,11]. Our theory, based on the H-cell RG, relates to the latter case. The numerical exception involves Neumann and Havlin's [11] data for the distribution of mass in 2D site percolation on a square lattice. On the other hand, except for the different normalization prefactor, one expects that the minimal path distribution (with fixed L) depends on the same scaled variable, $l/L^{d_{\min}}$, as the distribution of L's with fixed l, and it is reasonable to expect the same exponential factor in both distributions. We shall try to compare available numerical data for the minimal paths with our predictions below. Unfortunately, we are not aware of numerical data for the distribution of maximal paths, average edge-to-edge SAW, or the mass of the backbone, calculated with fixed geometrical distance.

We also discuss the distribution of the SCB, which is described by a supercritical branching process with $m=0$, and present a comparison with the numerical data [38]. This subsection is then concluded with a short discussion of the above comparisons.

1. Distribution of the mass of the cluster

For the mass distribution Ref. [11] assumed simple functional forms for $g(\omega)$ to analyze their data, like $\exp(C-A^{\dagger}\omega^{\delta'}-B^{\dagger}\omega^{\eta'})$ or $B^{\dagger}\omega^{\eta'}\exp(-A^{\dagger}\omega^{\delta'})$, finally settling to favor the former double-exponential form. In particular, they found that both trial functions gave $\delta'=19.2\pm 0.2$ for the right-hand tail.

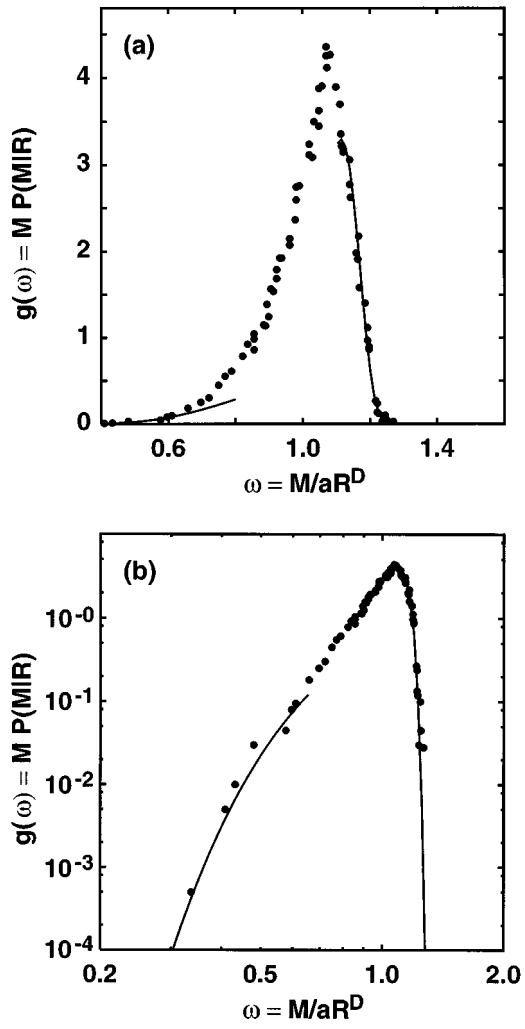

FIG. 6. Plot of the distribution of mass within radius R: $P(M|R)M=g(M/\langle M\rangle)=g(\omega)$ vs $M/aR^D=M/\langle M\rangle=\omega$ in (a) linear, (b) double-logarithmic scale (●). Data are taken from Fig. 7 in Ref. [11], and the distribution is normalized using $a=2.08$. Solid lines represent our suggested asymptotic behavior Eqs. (32) and (33) with $\eta'=1/(1-D)\approx-1.116$ and $\delta'=2/(2-D)=19.2$. The (near) constants $A^{\dagger}\approx0.12\pm0.04$ and $B^{\dagger}\approx4\pm2$ are fitted to the data.

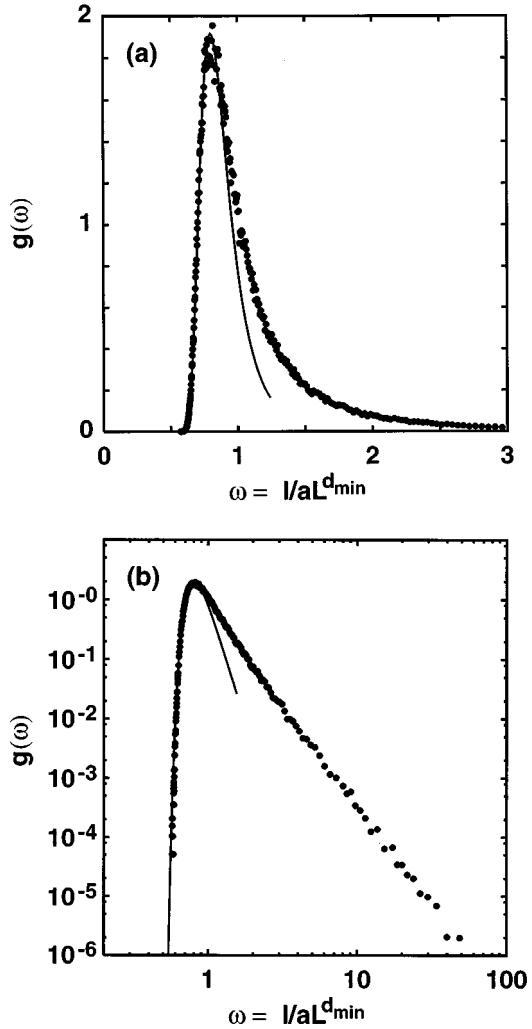

FIG. 7. The distribution of the lengths l of minimal paths for geometrical distance L: $g(\omega)$ versus $\omega=l/\langle l\rangle=l/aL^{d_{\min}}$ in (a) linear, (b) double-logarithmic scale. The data are from Ref. [37], and we find $a=0.805$. Solid lines represent our suggested asymptotic behavior Eq. (32) with $\eta'=1/(1-d_{\min})\approx-7.143$, $d_{\min}=1.14\pm0.01$ [11,22], and $B^{\dagger}=0.235\pm0.04$. The data apparently does not extend to the asymptotic regime on the right-hand end, and therefore comparison with Eq. (33) is not shown.

Analyzing the data from Ref. [11] we find that the amplitude reads $a=2.08\pm0.01$. Then, using Eqs. (37) and (38), we find that the exponents describing the tail behavior should read $\eta'=(1-D)^{-1}\approx-1.116$ and $\delta'=2/(2-D)=19.2$. The latter result is in agreement with Ref. [11], because the normalization affects only the coefficient $A^{\dagger}$. Since we do not know the exact f for the limit $L\to\infty$ [34], $A^{\dagger},B^{\dagger}>0$ as well as the prefactors $c'_{1,2}$ in Eqs. (32) and (33) have to be fitted. The result of this comparison is displayed in Fig. 6. We see that the asymptotic behavior of the data is indeed reasonably well described by the theoretical predictions in *both* ends. In particular, the fit on the right-hand tail is quite impressive, but allowing some inaccuracy for the last points on the left-hand tail would improve the fit also in that tail (see Fig. 4 of Ref. [17]). This agreement between the H-cell RG and the numerical data of Fig. 6 also supports the universality of g between the site and bond problems.

2. Distribution of the minimal paths

This distribution has been studied quite extensively during the last years. Usually it has been assumed [11,36] that the minimal path distribution has a simple power-exponential functional form, i.e., $g(\omega)=C\omega^{\gamma}\exp(-B^{\dagger}\omega^{\eta'})$, where heuristic arguments [10,36] give that $\eta'=(1-d_{\min})^{-1}$.

Figure 7 shows the distribution of minimal paths as measured from the 2D site problem on the square lattice [37]. Analyzing these data we find the amplitude $a=0.805\pm0.010$. The left-hand tail of this distribution essentially gives the probability for the minimal path being a straight line, and should behave according to Eq. (32) with $\eta'=(1-d_{\min})^{-1}\approx-7.143$. Note that the exponential term reproduces earlier heuristic arguments for this asymptotics [10], while (as discussed in Sec. IV A 2) the power-law prefactor $\omega^{\eta'-1}$ results from assuming only the simplest kind of correction, i.e., a constant, in Theorem 2. As shown in Fig. 7

the data fits excellently with this result. In fact, Eq. (32) seems to reproduce much of this distribution, even near the peak. On the other hand, using Eq. (33), the right-hand tail of this distribution should also decay exponentially, with $\delta' = 2/(2-d_{\min}) \approx 2.326$ for large $\omega = l/aL^{d_{\min}}$. However, the exponential term apparently dominates only very far in the right-hand tail. The available data for the right-hand tail look like a power law, thus being still in an intermediate range of ω. Therefore, we were not able to fit the right-hand tail of these data acceptably with Eq. (33).

3. Distribution of the singly connected bonds

The distribution of the number of the singly connected bonds has been discussed by Kantor [38], who measured this distribution from the 2D bond problem on the square lattice. In particular, the numerical measurements of Ref. [38] show that there is a finite probability to have no SCB, in the pleasing agreement with our RG results. In fact, the data give that this probability is about 0.19 [38], which practically coincides with the extrapolation of the H-cell RG results to large L, $q_{\mathrm{RG}} = 0.18 \pm 0.01$. This precise agreement is probably due to the fact that H-cell RG relates to the bond problem. In fact, q may depend on the specific percolation problem (e.g., lattice structure).

Figure 8 shows the distribution $\hat{g}$ for the number of the singly connected bonds. The solid lines in Fig. 8 show the predicted power-law (exponential) asymptotics for the left-hand (right-hand) tail of this distribution. The left-hand tail agrees very well with Eq. (34), although the best fit on that tail is achieved by choosing $\alpha' = 0.22 \pm 0.03$, which is slightly smaller than the RG estimate $\alpha'_{\mathrm{RG}} = 0.35 \pm 0.15$. However, taking into account that the RG estimate is based on extrapolation of the results from very small H cells with $L = 2,3,4$ to $L \to \infty$, this small numerical discrepancy is not significant. The right-hand tail seems to be also well described by Eq. (33), where $\delta' = 2/(2-d_{\mathrm{sc}}) = 8/5$. It is satisfactory to observe that the data agree with the RG predictions in *both* tails.

4. Discussion

In general, the above checks reveal that the RG predictions compare favorably with the numerical data from critical 2D percolation clusters. In particular, the distribution of SCB show excellent *quantitative* agreement with the RG calculations. On the other hand, the fit to the right-hand tail of the minimal path distribution is disappointing. As noted above, Eq. (32) seems to explain much of the available data of the minimal path distribution. This is probably due to the fact that $d_{\min}$ is close to unity, and, therefore, η' is large. On the other hand, it seems that the right-hand tail of Fig. 7 has not yet reached the other asymptotic regime governed by Eq. (33). Note that the numerical checks using RG distributions, for which Theorem 2 is definitely exact, already demonstrated that the asymptotic regime may apply only for very large (small) arguments. Since more precise measurements of the right end of the minimal path distribution may demand more computer time than what is feasible today, additional checks for other distributions, like that of (average, longest) SAW or the mass of the backbone, seem highly desirable.

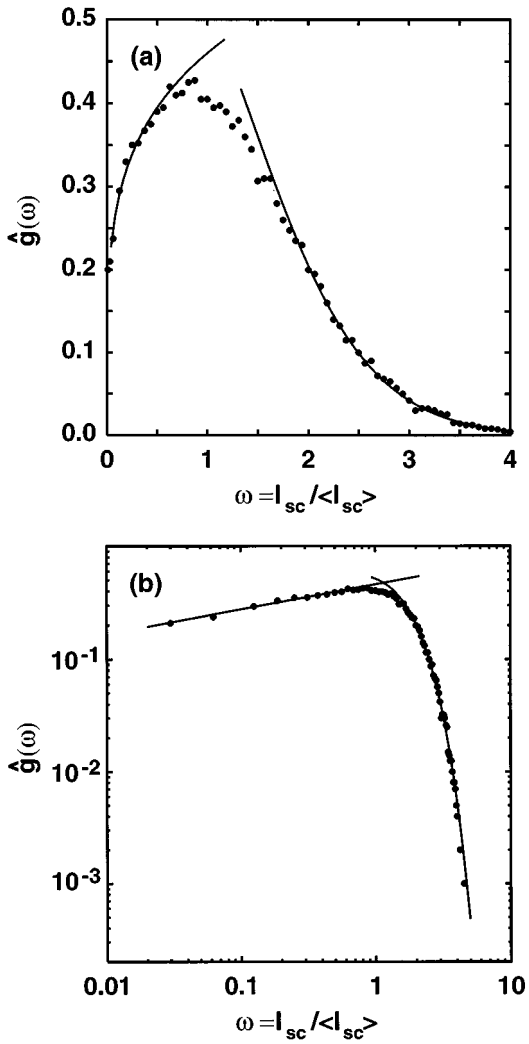

FIG. 8. The conditional distribution of the number of the singly connected bonds: $\hat{g}(\omega)$ vs $\omega = l_{\mathrm{sc}}/\langle l_{\mathrm{sc}}\rangle$ in (a) linear, (b) double-logarithmic plot. The data are taken from Ref. [38]. The solid lines show the predicted asymptotic behavior Eqs. (34) and (33) with $\delta' = 2/(2-d_{\mathrm{sc}}) = 8/5$. Here $\alpha' = 0.22 \pm 0.03$ and $A^{\dagger} = 0.66 \pm 0.2$ are fitted to the data.

However, to the best of our knowledge, such measurements with fixed geometrical distance do not exist presently.

For simplicity, we have concentrated on 2D percolation, but our results can be straightforwardly generalized to general d dimensions. Considering a d-dimensional H cell, it is easy to observe that the structure of the generating functions f remains unchanged, except for the generalization in $M \approx L^d$ [see Eq. (17)]. Thus, with the exception of SCB, the asymptotic tail behavior is still given (at least within exponential accuracy) by Eqs. (32) and (33), with

$$\eta' = (1-\tilde{D})^{-1}, \tag{39}$$

$$\delta' = d/(d-\tilde{D}). \tag{40}$$

For the distribution of SCB there should be a nonzero probability q to find no SCB ($d < 6$), and Eqs. (34) and (33) apply with $\delta' = d/(d-d_{\mathrm{sc}})$. Our theory does not give the functional forms of $\alpha'(d), q(d)$.

D. Localized wave functions and Ising spin correlations

In order to illustrate the applications of the above results, we discuss the moments of localized wave functions and Ising spin correlations, which couple to the minimal path and SCB distributions, respectively. Although the minimal path and SCB distributions are both unifractal, i.e., $\langle l^k\rangle \propto L^{kd_{\min}}$, the physical properties which depend on them may show multifractal features.

1. Moments of localized wave functions

As noted above, the localized wave function $\Psi \propto \exp(-l/\xi)$ [1], where ξ is the localization length. Recently, Ref. [2] studied these localized excitations on the critical percolation clusters by assuming the power-exponential form for the minimal path distribution, $g(\omega)=C\omega^{\gamma}\exp(-B^{\dagger}\omega^{\eta'})$. Using steepest descents, these authors found that the moments of Ψ behave as

$$\ln\langle \Psi^k\rangle \propto k^{(1/d_{\min})}L, \quad \text{for } 0<k<k_{c,1}, \tag{41}$$

$$\ln\langle \Psi^k\rangle \propto \text{const}+kL, \quad \text{for } k>k_{c,1}>0, \tag{42}$$

where $k_{c,1}=-B^{\dagger}\eta'\xi$, and in this case L denotes the distance from the center of the localized excitation. The unifractal behavior above $k_{c,1}$ arose because of the constraint $l>L$. Although their numerics supported the multifractality of Eq. (41), they could not collect numerical evidence for the crossover to unifractal behavior, Eq. (42), for $k>k_{c,1}$.

Now we apply the mathematical results of Sec. III to analyze these moments of Ψ. From the exponential decay of the wave function, $\Psi\propto\exp(-l/\xi)$, and Eq. (18) if follows that

$$\langle \Psi^k\rangle = \langle e^{-kl/\xi}\rangle = \langle e^{-(k\langle l\rangle/\xi)l/\langle l\rangle}\rangle = \phi\left(-\frac{k\langle l\rangle}{\xi}\right). \tag{43}$$

For illustration, see Fig. 2 which shows ϕ from the 2×2 H cell. Using Theorem 1, for $L\to\infty$, we find

$$\ln\langle \Psi^k\rangle = c_1 + A\left|\left(\frac{k\langle l\rangle}{\xi}\right)\right|^{\delta} = c_1 + c_2|k|^{(2/d_{\min})}L^2, \quad \text{as} \quad k\to-\infty, \tag{44}$$

$$\ln\langle \Psi^k\rangle = c_1' - B\left(\frac{k\langle l\rangle}{\xi}\right)^{\eta} = c_1' + c_2' k^{(1/d_{\min})}L, \quad \text{as } k\to\infty, \tag{45}$$

with constants c_1, c_2, c_1', and c_2'.

Up to this point, we have considered the behavior of the physical properties in the limit $L\to\infty$. However, in this context L plays the role of the distance from the center of the fraction instead of the system size. In order to take into account the effects of finite L, we have to consider necessary modifications of Eq. (18). Since the lengths of the minimal paths have lengths between L and L^2 [see Eq. (10)], ω is bounded by $\omega_{\min}\le\omega\le\omega_{\max}$ with $\omega_{\min}=L/\langle l\rangle = (1/a)L^{1-d_{\min}}$ and $\omega_{\max}\approx L^2/\langle l\rangle=(1/a)L^{2-d_{\min}}$. In this case Eq. (18) need to be replaced by

$$\phi_L(s)=\int_{\omega_{\min}}^{\omega_{\max}} e^{\omega s} g(\omega)\,d\omega. \tag{46}$$

In particular, if $s=-k\langle l\rangle/\xi$, then for large enough k the integrand is largest at $\omega=\omega_{\min}$ and decays fast for larger ω. Using Eq. (32) we find that this happens for $k>k_{c,1}\equiv -B^{\dagger}\eta'\xi a^{\eta'-1}$. Thus for $k>k_{c,1}$ the moments of Ψ depend on the lower integration bound

$$\begin{aligned}\ln\langle \Psi^k\rangle &= \ln\left[\int_{\omega_{\min}}^{\omega_{\max}} e^{-k\langle l\rangle\omega\xi} g(\omega)\,d\omega\right]\\ &\approx \ln[g(\omega_{\min})e^{-kL/\xi}]\\ &= c - kL/\xi, \quad \text{for } k>k_{c,1},\end{aligned} \tag{47}$$

where c is a constant. This calculation thus reproduces Eq. (42). Similarly, for $k<k_{c,2}\equiv -A^{\dagger}\delta'\xi a^{\delta'-1}$, the integral is dominated by the upper cutoff. In this case

$$\begin{aligned}\ln\langle \Psi^k\rangle &= \ln\left[\int_{\omega_{\min}}^{\omega_{\max}} e^{-k\langle l\rangle\omega/\xi} g(\omega)\,d\omega\right]\\ &\approx \ln[g(\omega_{\max})e^{-kL^2/\xi}]\\ &= c' - kL^2/\xi, \quad \text{for } k<k_{c,2},\end{aligned} \tag{48}$$

with a constant c'.

In conclusion, we find that both the negative and positive moments are multifractal for large $|k|$ and $k_{c,2}<k<k_{c,1}$. However, for large enough $|k|$, the moments of Ψ are determined by the distance of shortest or longest minimal path instead of the distribution $g(\omega)$. This gives that high moments of Ψ are unifractal [see Eqs. (47) and (52)]. The results for positive moments were previously obtained in Ref. [2], while the considerations of the negative moments are new. These negative moments are dominated by the very rare small values of Ψ.

2. Moments of Ising spin correlations

At low temperatures, Ising spin correlations behave as $\overline{S_0S_L}\propto\exp(-l_{\rm sc}/\xi)$ [3], where the overline denotes the thermal averaging and ξ is the spin-spin correlation length. Similarly to the localized wave functions, we have

$$\begin{aligned}\langle \overline{S_0S_L}\rangle &= \langle \exp(-kl_{\rm sc}/\xi)\rangle\\ &= \langle e^{-(k\langle l_{\rm sc}\rangle/\xi)l_{\rm sc}/\langle l_{\rm sc}\rangle}\rangle = \phi\left(-\frac{k\langle l_{\rm sc}\rangle}{\xi}\right),\end{aligned} \tag{49}$$

and therefore, using Theorem 1,

$$\ln\langle \overline{S_0S_L}\rangle = c_1 + A\left|\frac{k\langle l_{\rm sc}\rangle}{\xi}\right|^{\delta} = c_1 + c_2|k|^{(2/d_{\rm sc})}L^2, \quad \text{as } k\to-\infty, \tag{50}$$

$$\ln\langle \overline{S_0S_L}\rangle = c_1' + B\left(\frac{k\langle l_{\rm sc}\rangle}{\xi}\right) = c_1' + c_2' kL^{d_{\rm sc}}, \quad \text{as } k\to\infty, \tag{51}$$

with constants c_1, c_2, c_1', and c_2'.

In this case finite L introduces only an upper cutoff to Eq. (18), since $0<\omega\le\omega_{\max}\approx L^2/\langle l_{\rm sc}\rangle=(1/a)L^{2-d_{\rm sc}}$. Therefore, for $k<k_{c,2}\equiv -A^{\dagger}\delta'\xi a^{\delta'-1}$,

$$\ln\langle \overline{S_0 S_L} \rangle = \ln\left[\int_0^{\omega_{\max}} e^{-k(\langle l_{sc} \rangle \omega/\xi} g(\omega) d\omega \right]$$
$$\approx \ln[g(\omega_{\max}) e^{-kL^2/\xi}] = c' - kL^2/\xi, \quad \text{for } k < k_{c,2}, \tag{52}$$

where c' is a constant.

In conclusion, we find that the positive moments of the Ising spin correlation are unifractal for large k. On the other hand, the negative moments are multifractal for large $|k|$ and $k > k_{c,2}$, but cross over to the unifractal behavior for $k < k_{c,2}$.

V. CONCLUSIONS AND DISCUSSION

We have studied the distributions of the structural properties for percolation clusters between two terminals at a fixed geometrical distance, using the H-cell renormalization group. We showed that this RG is equivalent to a branching process, and applied the tools developed in the mathematical literature to obtain results for the distribution functions, which are exact on the hierarchical lattice and approximate for the original square lattice. This approach strongly supports scaling functions as in Eq. (1), which depend only on the scaled variable, e.g., $l/\langle l \rangle$.

We found that the mapping between branching processes and RG is applicable for *general* unifractal distributions encountered in percolation. We computed the distributions of the minimal and maximal paths, the average edge-to-edge SAW; the number of the singly connected bonds, the number of spanning clusters, and the masses of the percolation clusters as well as it's backbone. We derived recursion relations for these distribution functions, and found exact functional forms for their asymptotic tail behavior at both small and large arguments in *general* dimension d.

Our predictions for the asymptotic tail behavior were numerically checked using published data from 2D percolation clusters. In general, our results agree well with the available numerical data, but the results for the large argument tail of the minimal path distribution were disappointing probably due to the insufficient numerics. On the other hand, the RG results for the number of singly connected bonds are *quantitatively* supported by the numerical data. Thus we hope that this paper stimulates more numerical work for other distributions, like simulations for distributions of the (average, longest) SAW or the mass of the backbone, to check our predictions in more detail.

We also obtained some results for the distribution of localized wave functions as well as for the Ising spin correlations. We find that the kth moments of these properties are multifractal for large $|k|$, except for large positive moments of Ising spin correlations which are unifractal. However, ultimately for large enough $|k|$ all these moments cross over to unifractal behavior. We find that these high moments are determined by the integration limits instead of by $g(\omega)$.

In particular, we found encouraging results for the number of singly connected bonds where most accurate mathematical information is available. Apparently, more detailed mathematical knowledge of supercritical branching processes, with $m > 1$, would enable more accurate predictions also for other structural properties for percolation. While this information may be available in the future, we hope that this work combining the RG with branching processes may ultimately show a way to an exact calculation of these distributions.

In all the examples we treated only geometrical properties involving substructures of a *single* cluster which connects two terminals. This is an artifact of the hierarchical structure, which consistently treats each smaller part of the cluster as connecting two end points of the corresponding Wheatstone bridge. One can imagine other RG schemes, which would allow breaking the cluster into disjoint parts so that each part still connects the two opposite edges of the sample. In such a RG scheme one could derive generating functions for the number of spanning clusters, a topic which has recently attracted much attention [39]. Below six dimensions, one expects the average number of spanning clusters to remain finite, hence $\mu = 1$. Theorems for such *critical* branching processes predict that $g(\omega)$ decays exponentially with ω, [40,41] in apparent contradiction to Aizenman's proof that $g(\omega)$ should be exponential in ω^2 [39], as also recently confirmed numerically [42,43]. We hope that future work will clarify this apparent contradiction.

ACKNOWLEDGMENTS

We thank J. D. Biggins and N. H. Bingham for correspondence about the mathematical work on branching processes, H. E. Roman for communicating his data for the minimal path distribution to us, M. Aizenman for discussions on the number of spanning clusters, and D. Stauffer and P. Sen for comments on the manuscript. J.-P.H. gratefully acknowledge financial support from the Neste Foundation, Emil Aaltonen Foundation, and the Finnish Cultural Foundation. This project was also supported by grants from the U.S.-Israel Binational Science Foundation (BSF) and the German-Israeli Foundation (GIF).

[1] A. B. Harris and A. Aharony, Europhys. Lett. **4**, 1355 (1987).
[2] A. Bunde, H. E. Roman, S. Russ, A. Aharony, and A. B. Harris, Phys. Rev. Lett. **69**, 3189 (1992).
[3] A. Aharony, Y. Gefen, and Y. Kantor, J. Stat. Phys. **36**, 795 (1984).
[4] B. B. Mandelbrot and J. A. Given, Phys. Rev. Lett. **52**, 1853 (1984).
[5] D. Stauffer and A. Aharony, *Introduction to Percolation Theory*, revised 2nd ed. (Taylor and Francis, London, 1994).
[6] B. B. Mandelbrot, *The Fractal Geometry of Nature* (Freeman, San Fransisco, 1982).
[7] A. Kapitulnik, A. Aharony, G. Deutscher, and D. Stauffer, J. Phys. A **16**, L269 (1984).
[8] J.-P. Hovi, A. Aharony, D. Stauffer, and B. B. Mandelbrot, Phys. Rev. Lett. **77**, 877 (1996).
[9] S. Havlin and R. Nossal, J. Phys. A **17**, L427 (1984).

[10] S. Havlin, B. L. Trus, G. H. Weiss, and D. Ben-Avraham, J. Phys. A **18**, L247 (1985).
[11] A. U. Neumann and S. Havlin, J. Stat. Phys. **52**, 203 (1988).
[12] D. Lhuiller, J. Phys. (France) **49**, 705 (1988).
[13] A. K. Roy and A. Blumen, J. Stat. Phys. **59**, 1581 (1990).
[14] P. J. Reynolds, H. E. Stanley, and W. Klein, J. Phys. C **10**, L167 (1977).
[15] J. Bernasconi, Phys. Rev. B **18**, 2185 (1978).
[16] A. Aharony, E. I. Hinrichsen, A. Hansen, J. Feder, T. Jøssang, and H. H. Hardy, Physica A **177**, 260 (1991).
[17] J.-P. Hovi and A. Aharony, Fractals **3**, 453 (1995).
[18] P. Le Doussal and J. Machta, J. Stat. Phys. **64**, 541 (1991).
[19] J.-P. Hovi and A. Aharony, J. Stat. Phys. **86**, 1163 (1997).
[20] D. C. Hong and H. E. Stanley, J. Phys. A **16**, L475 (1983).
[21] A. Coniglio, Phys. Rev. Lett. **46**, 250 (1981).
[22] H. J. Herrmann and H. E. Stanley, J. Phys. A **21**, L879 (1988).
[23] K. Y. Woo and S. B. Lee, Phys. Rev. A **44**, 999 (1991).
[24] P. Grassberger, J. Phys. A **26**, 1023 (1993).
[25] M. D. Rintoul, J. Moon, and H. Nakanishi, Phys. Rev. E **49**, 2790 (1994).
[26] P. Grassberger, J. Phys. A **25**, 5475 (1992).
[27] T. E. Harris, *The Theory of Branching Processes* (Springer, Berlin, 1963); K. B. Athreya and P. E. Ney, *Branching Processes* (Springer, Berlin, 1972).
[28] H. W. Watson and F. Galton, J. Anthropol. Inst. Great Britain Ireland **4**, 138 (1874).
[29] T. E. Harris, Ann. Math. Stat. . **41**, 474 (1948).
[30] N. H. Bingham, J. Appl. Probab. **25A**, 215 (1988).
[31] J. D. Biggins and N. H. Bingham, Adv. Appl. Probab. **25**, 757 (1993).
[32] S. Dubuc, Z. Wahrscheinlichkeitstheor. Verwandte Geb. **19**, 281 (1971).
[33] J. D. Biggins and N. H. Bingham, Math. Proc. Camb. Philos. Soc. Soc. **110**, 545 (1991).
[34] The periodic functions of Theorems 1 and 2 are completely determined by f [29]. Thus, their determination in the small cell RG calculations does not involve any fitting of the data.
[35] The correction terms to the exponential decay, form an active mathematical problem in it's own right. [J. D. Biggins and N. H. Bingham (private communication).]
[36] A. Aharony and A. B. Harris, Physica A **191**, 365 (1992).
[37] H. E. Roman (private communication). The original data are calculated for fixed topological distance, which yields the distribution as function of $\tilde{\omega}=L/\langle L\rangle \propto L/l^{(1/d_{\min})}$. Assuming that the leading exponential terms are the same as for fixed Euclidean distance, the data shown in Fig. 7 are calculated by changing variables.
[38] Y. Kantor, J. Phys. A **19**, L497 (1986).
[39] M. Aizenman, Nucl. Phys. B **445**, 551 (1997).
[40] A. M. Yaglom, Doklady **56**, 795 (1947).
[41] R. S. Slack, Z. Wahrscheinlichkeitstheor. Verwandte Geb. **9**, 139 (1968).
[42] P. Sen, Int. J. Mod. Phys. **7**, 603 (1996).
[43] C. K. Hu and C. Y. Lin, Phys. Rev. Lett. **77**, 8 (1996).